Numerical Study of Heat Transfer from Elliptic Tube in a Fluidized Bed

M. A. Abd-Rabbo[1], R. Y. Sakr[2], M. A. Mohammad[1] and M. M. Mandour[2*]

[1]*Department of Mechanical Engineering, Faculty of Engineering, Al-Azhar University, Egypt.*
[2]*Department of Mechanical Engineering, Faculty of Engineering Shoubra, Benha University, Egypt.*

Authors' contributions

This work was carried out in collaboration among all authors. Authors MAAR and RYS designed the study, performed the statistical analysis and wrote the protocol. Author MAM managed the analyses of the study. Author MMM wrote the first draft of the manuscript and managed the literature searches. All authors read and approved the final manuscript.

Original Research Article

ABSTRACT

In the present work, heat transfer characteristics and flow field from a heated elliptic cylinder immersed in fluidized bed is studied numerically using CFD package. The flow pattern and heat transfer fields around the heated cylinder is predicted using a two fluid Eulerian-Eulerian model coupled with kinetic theory of granular flow (KTGF) with heat transfer. Experiments were carried out under uniform heat flux condition, with air as a fluidizing gas and pulverized coal as a bed material. The Reynolds number based on the equivalent hydraulic diameter, D_h, was ranged from 941to 1263. The simulation results of the present study showed that, for the range of gas velocity considered, at minimum fluidization velocity, Re = 914, the Nu_θ is maximum at the sides of the cylinder and minimum at the stagnation, $\theta=0^o$, and top, $\theta=180^o$, of the cylinder. The average Nusselt number for the elliptic cylinder increases with the increase of the fluidization velocity. The present data is compared with a previous well-known correlation from the literature for a circular cylinder and a reasonable deviation about 11-30% is found.

Keywords: Heat transfer; CFD; elliptic cylinder; fluidized bed.

_____

Corresponding author: Email: mustafamandour@yahoo.com;

NOMENCLATURE

A_c : Cross-sectional area of heated cylinder, m^2;
A_s : Surface area of heated cylinder, m^2;
D : Reactor width, m;
H : Reactor height, m;
h : heat exchange;
h_0 : Static bed height of solid, m;
D_h : Hydraulic diameter of elliptic cylinder, m;
P : Pressure, kg/m^2;
p : The perimeter of the tested cylinder, m;
Nu_p : Average nusselt number, based on particles diameter;
Nu_θ : Local nusselt number;
U_{sup} : Superficial air velocity, m/s;
U_{mf} : Minimum fluidization velocity, m/s;
Re : Reynolds number;
FBR : Fluidized bed reactor;
CFD : Computational fluid dynamics;
TFM : Two fluid models;
$KTGF$: Kinetic theory for granular flow;
ε : volume fraction;
K_{gs} : Gas-solid momentum exchange coefficient;
ρ : Density;
υ : Local velocity;
$\overline{\overline{\tau}}_s$: Stress tensor;
μ : Viscosity;
K^{eff} : Effective thermal conductivity;
$\emptyset_{gs}$: ENERGY change between the gas or solid phases;
K_{θ_s} : The diffusion coefficient;
γ_{θ_s} : The collisional dissipation of energy;
g_0 : The radial distribution function;
θ_s : Granular temperature;

SUBSCRIPTS

θ : Local angle in the axial direction;
a : Air;
b : Bulk;
s : Cylinder's surface;
c : Cylinder's cross-section;
g : Gas phase;
s : Solid phase;
col : Collision;
fr : Friction;
kin : Kinetic;
mf : Minimum fluidization;

1. INTRODUCTION

Fluidization is the phenomenon of transferring fluid properties to solid particles of a bed via passing a fluid through this bed. This technology can be used in different applications such as chemical, biochemical and petrochemical industries. Because they are characterized by uniformity of temperature distribution and high rates of heat transfer, due to the intense mixture of the solid material by the presence of gas bubbles. Heat transfer and fluid flow around immersed surfaces in packed and fluidized beds have been the focus of a variety of numerical, experimental studies and modelling efforts. The influences of different parameters affect these regimes (eg., thermal conductivity, static height of bed, bed particles diameter/ type, Superficial fluidization velocity, bubbling, etc) have been studied and presented extensively by the majority of researchers in the fluidization literature.

Kuipers et al., [1] developed a gas-fluidized bed model based on "two-fluid model", TFM, to measure the pressure, the porosity, the temperature of the fluid and solid phases, and the velocity fields of both phases. Gustavsson and Almstedt, [2] developed a TFM solver to simulate the fluid dynamics of bubbling in fluidized beds with two internal horizontal heat exchanger tubes. The used numerical code, Gemini, was based on the implicit multi-field method (IMF) of Harlow and Amsden for Eulerian two-fluid modelling, assuming no turbulence in the gas or solid phase. Yusuf et al., [3] studied the effect of particle size and gas velocity on heat transfer coefficient between a heated wall to gas-fluidized bed using the 2-D Eulerian-Eulerian approach. Simulation of a bubbling bed was carried out on the in-house code FLOTRACS-MP-3D. Wankhede and Adgulkar, [4] studied the CFD simulations of heat transfer from the immersed small tube in a two-dimensional fluidized bed of different material with different particle diameter. The bubbling fluidized bed simulations were performed using FLUENT 6.0, a commercial finite volume code. Zhao et al., [5] conducted simulations using the combined Computational Fluid Dynamics-Discrete Element Method (CFD-DEM) to analyse particle-particle and particle-fluid heat transfer behaviours by quantifying the contribution to heat transfer coefficient via convection, conduction, and radiation. Armstrong et al., [6] modelled one, two and three heated tubes immersed in fluidized bed reactors using an Eulerian–Eulerian kinetic theory of granular flow model. Teaters, [7] used a (CFD) with and without turbulence modelling to predict the gas-solid hydrodynamics of fluidized beds. He studied a single solids phase glass bead and walnut shell fluidized beds to show the

distinction between different flow regimes, bubbling, slugging, and turbulent. Perrone and Amelio [8] studied the hydrodynamics and heat transfer from a heated wall to a fluidized bed using the Eulerian–Eulerian approach. They used the CFD technique to understand the behaviour of gas-solid flow and the bubbles production. Schmidt and Renz [9] investigated numerically the heat transfer between a fluidized bed's particles of Geldart B classification and an immersed tube. The results analysed the impact of the bed hydrodynamics on heat transfer coefficients. Gan et al. [10] applied CFD-DEM to study the effect of sphericity of particles on the heat transfer behaviour in fluidized beds. They found that, spherical particles had lower effective thermal conductivity than ellipsoidal particles. Wahyudi et al. [11] conducted 3-D simulations to study hydrodynamics and heat transfer behaviour of a fluidized bed with an immersed tube using CFD-DEM. Li et al., [12] used a (CFD-DEM) model to simulate heat transfer in a pseudo-2D fluidized bed with heat production in the particle phase. Most studies to date have focused on heat transfer between bed material and surfaces immersed in it. These immersed surfaces are often cylinders with circular cross section although there are many researchers proved that, the cylinders with non-circular cross section especially elliptic ones have good aerodynamic characteristics better than that in circular ones.

2. CFD SIMULATION

Interactions between gas and solids phases are achieved due to the high particle concentrations in fluidized beds. In fact, the fluidized solids have similar properties as a continuous fluid. Therefore, the Eulerian approach is a good tool for the numerical simulation of fluidized beds. This model allows for the presence of two different phases in one control volume of the grid by introducing the volume fraction variable. The viscous forces and the solid pressure of the particle phase can be described by using the kinetic theory of granular flows, as a function of the so-called granular temperature.

3. GOVERNING EQUATIONS

The following governing and Constitutive equations were solved using computational fluid dynamics ANSYS Fluent 14.5 to predict the bed hydrodynamics of pulverized coal. Gas phase, air, was considered to be the primary phase, while solid phase, pulverized coal, was considered to be secondary or dispersed phase. For this purpose, the phase coupled SIMPLE scheme which is an extension of the SIMPLE algorithm to multiphase flows was used to consider the pressure–velocity coupling. Moreover, the second order upwind discretization schemes were used for the volume fraction and momentum terms.

3.1 Governing Equations for Flow and Heat Transfer in a Fluidized Bed Reactor

3.1.1 Volume fraction equation

$$\varepsilon_g + \varepsilon_s = 1$$

3.1.2 Conservation of mass, continuity equation

Gas: $\frac{\partial(\varepsilon_g \rho_g)}{\partial t} + \nabla.\left(\varepsilon_g \rho_g \vec{v}_g\right) = 0$

Solid: $\frac{\partial(\varepsilon_s \rho_s)}{\partial t} + \nabla.\left(\varepsilon_s \rho_s \vec{v}_s\right) = 0$

where ε, ρ and v are the volume fraction, density and local velocity, respectively.

3.1.3 Conservation of momentum

Gas: $\frac{\partial(\varepsilon_g \rho_g \vec{v}_g)}{\partial t} + \nabla.\left(\varepsilon_g \rho_g \vec{v}_g \vec{v}_g\right) = -\varepsilon_g \nabla P + \nabla.\bar{\bar{\tau}}_g + \varepsilon_g \rho_g \vec{g} + K_{gs}(\vec{v}_g - \vec{v}_s)$

Solid: $\frac{\partial(\varepsilon_s \rho_s \vec{v}_s)}{\partial t} + \nabla.\left(\varepsilon_s \rho_s \vec{v}_s \vec{v}_s\right) = -\varepsilon_s \nabla P - \nabla P_s + \nabla.\bar{\bar{\tau}}_s + \varepsilon_s \rho_s \vec{g} + K_{gs}(\vec{v}_g - \vec{v}_s)$

Where K_{gs} is the gas-solid momentum exchange coefficient, ρ is gas phase static pressure, ρ_s is solid pressure and g and $\bar{\bar{\tau}}_s$ are the gravity acceleration and stress tensor, respectively.

3.1.3.1 The stress tensors

Gas: $\bar{\bar{\tau}}_g = \varepsilon_g \mu_g \nabla.\vec{v}_g + 2\varepsilon_g \mu_g \nabla.\vec{v}_g^T - \frac{2}{3}\varepsilon_g \mu_g \nabla.\vec{v}_g I$

Solid: $\bar{\bar{\tau}}_s = \varepsilon_s \mu_b \nabla.\vec{v}_s I + \varepsilon_s \mu_s \nabla.\vec{v}_s + 2\varepsilon_s \mu_s \nabla.\vec{v}_s^T - \frac{2}{3}\varepsilon_s \mu_s \nabla.\vec{v}_s I$

Where μ_b, μ_g and μ_s are granular bulk, gas and solid viscosities, respectively.

3.1.4 Conservation of energy

Gas: $\frac{\partial(\varepsilon_g \rho_g H_g)}{\partial t} + \nabla.\left(\varepsilon_g \rho_g \vec{v}_g H_g\right) = \nabla.\varepsilon_g K_g^{eff} \nabla T_g - h_{gs}(T_s - T_q)$

Solid: $\frac{\partial(\varepsilon_s \rho_s H_s)}{\partial t} + \nabla.\left(\varepsilon_s \rho_s \vec{v}_s H_s\right) = \nabla.\varepsilon_s K_s^{eff} \nabla T_s - h_{sg}(T_s - T_g)$

Where H_g and H_s are specific enthalpy, K_g^{eff} and K_s^{eff} are effective thermal conductivity for gas and solid phases and h_{gs} is the heat exchange between the gas and solid phases, respectively.

3.2 Constitutive Equations Used to Close the Governing Equations

3.2.1 Syamlal O'Brien drag model

$$K_{gs} = \frac{3}{4} \frac{\varepsilon_s \varepsilon_g \rho_g}{v_{t,s}^2 d_s} C_D \left(\frac{Re_s}{v_{r,s}}\right) |\vec{v}_s - \vec{v}_g|$$

$$C_D = \left(0.63 + \frac{4.8}{\sqrt{Re_s v_{r,s}}}\right)^2$$

$$v_{r,s} = 0.5 \left(A - 0.06 Re_s + \sqrt{(0.06 Re_s)^2 + 0.12 Re_s(2B - A) + A^2}\right)$$

$A = \varepsilon_g^{4.14}$, $B = \varepsilon_g^{2.65}$ for $\varepsilon_g > 0.85$

$A = \varepsilon_g^{4.14}$, $B = 0.8\varepsilon_g^{1.28}$ for $\varepsilon_g \leq 0.85$

3.2.2 Kinetic fluctuation energy

$$\frac{3}{2}\left[\frac{\partial}{\partial_t}(\rho_s \varepsilon_s \theta_s) + \nabla \cdot (\rho_s \varepsilon_s \vec{v}_s \theta_s)\right] = (-\rho_s \bar{I} + \bar{\bar{\tau}}_s) : \nabla \cdot \vec{v}_s + \nabla \cdot (K_{\theta_s} \nabla \theta_s) - \gamma_{\theta_s} + \emptyset_{gs}$$

$$\gamma_{\theta_s} = \frac{12(1-e)^2 g_0}{d_s \sqrt{\pi}} \varepsilon_s^2 \rho_s \theta_s^{3/2} \qquad \emptyset_{gs} = -3K_{gs}\theta_s$$

$$K_{\theta_s} = \frac{15 d_s \rho_s \varepsilon_s \sqrt{\theta_s \pi}}{4(41 - 33\eta)}\left[1 + \frac{12}{5}\eta^2(4\eta - 3)\varepsilon_s g_0 + \frac{16}{15\pi}(41 - 33\eta)\eta\varepsilon_s g_0\right]$$

$$\eta = \frac{1}{2}(1 + e)$$

Where $(-\rho_s\bar{I} + \bar{\bar{\tau}}_s) : \nabla \cdot \vec{v}_s$ is the generation of energy by the solid tensor, $K_{\theta_s}\nabla\theta_s$ is the diffusion of energy while the term of K_{θ_s} is the diffusion coefficient, γ_{θ_s} is the collisional dissipation of energy, g_0 is the radial distribution function, and $\emptyset_{gs}$ is the energy change between the gas or solid and solid phases.

3.2.3 Solid shear viscosity

$$\mu_s = \mu_{s,col} + \mu_{s,skin} + \mu_{s,fr}$$

3.2.3.1 Collisional viscosity

$$\mu_{s,col} = \frac{4}{5}\varepsilon_s d_s \rho_s g_0(1 + e)\left(\frac{\theta_s}{\pi}\right)^{1/2}$$

3.2.3.2 Kinetic viscosity

$$\mu_{s,skin} = \frac{10 d_s \rho_s \sqrt{\theta_s \pi}}{96\varepsilon_s g_0(1 + e)}\left[1 + \frac{2}{5}\varepsilon_s g_0(1 + e)(3e - 1)\right]$$

3.2.3.3 Frictional viscosity

$$\mu_{s,fr} = \frac{\rho_s \sin\emptyset}{2\sqrt{I_{2D}}}$$

3.2.3.4 Solid bulk viscosity

$$\lambda_s = \frac{4}{3}\varepsilon_s d_s \rho_s g_0(1 + e)\left(\frac{\theta_s}{\pi}\right)^{1/2}$$

3.2.3.5 Particle pressure

$$P_s = \varepsilon_s \rho_s \theta_s + 2\rho_s(1 + e)\varepsilon_s^2 g_0 \theta_s$$

3.2.3.6 Radial distribution function

$$g_0 = \left[1 - \left(\frac{\varepsilon_s}{\varepsilon_{s,max}}\right)^{1/3}\right]^{-1}$$

Where θ_s is the granular temperature, g_0 is the radial distribution function and e is the restitution coefficient. The radial distribution function g_0 is related to probability of collisions between grains when the solid granular phase becomes dense. The restitution coefficient e is proportional to the energy loss in particle-particle collision. Its value is unity and zero for elastic and in-plastic collisions, respectively. The value of 0.9 was chosen in this study.

3.3 Particle Phase Boundary Conditions

3.3.1 Velocity

$$\vec{u}_{s,w} = -\frac{6\mu_s \varepsilon_{s,max}}{\sqrt{3}\sqrt{0}\pi\varphi\rho_s \varepsilon_s g_0}\frac{\partial\vec{v}_{s,w}}{\partial n}$$

3.3.2 Granular temperature

$$\theta_s = -\frac{K_{\theta_s}}{\gamma_w}\frac{\partial\theta}{\partial n} + \frac{\sqrt{3}\pi\varphi\rho_s\varepsilon_s g_0\vec{v}_{s,slip}^2\theta^{3/2}}{6\gamma_w\varepsilon_{s,max}}$$

$$\gamma_w = \frac{\sqrt{3}\pi(1 - e_w^2)\rho_s\varepsilon_s g_0\theta^{3/2}}{4\varepsilon_{s,max}}$$

4. MODEL SET-UP

Two dimensional rectangular bed reactor (D= 0.2 m, H= 1.5) is used as a numerical simulation model, as shown in Fig. (1-a), to reduce the solution time. The static head of the bed, h_0, is 0.25 m and air is introduced as a fluidizing gas through the domain inlet while the outlet is considered as pressure outlet and the other boundaries are considered as walls. The gas phase is considered to be no slip condition while

the solid phase is allowed to slip partially on walls. The gas and solid phases are set to the atmospheric temperature of 25°C. Wall heat flux for heating cylinder is assumed to be constant at 13.3 KW/m^2. The simulations were performed for 24000 time steps with a time step size of 0.00025 s to ensure quick convergence with a maximum of 20 iterations per time step and the simulation was run for 6 s of real time. For more details see Tables (1) and (2) which summarize numerical parameters used in the simulation. Multiphase Eulerian-Eulerian model is used to simulate the gas-solid flow. Conservation equations for each phase are derived to obtain a set of equations of the similar structure. In granular flows, the kinetic theory is applied to close these equations while the interaction between gas and solid phases is modelled using Syamlal O'Brien drag model [13]. The transient computational model was created in CFD software, FLUENT 14.5. The phase coupled SIMPLE algorithm along with second order upwind scheme has been used to solve the transport equations using the finite volume approach.

To perform grid sensitivity analysis and obtain optimum accuracy and computational time, grid sizes of 1 mm, 2 mm, and 5 mm are examined in the present work. A uniform mesh has been generated as shown in Fig. (1-b). Structured meshing method is used for meshing the geometry. In the present study, quadrilateral cells are used to mesh the general area of the column with a uniform cell size of 2 mm. The cell size in the region near the heated wall varied from 0.02 mm to 2 mm within increasing factor of 1.22 from the heated wall to obtain the local temperature gradients.

5. RESULTS AND DISCUSSION

Heat transfer from elliptic cylinder immersed in fluidized bed in addition to flow pattern are investigated numerically within the Reynolds number range of 914≤ Re ≤1263. The dimensionless coefficients, Nu and Re numbers have been calculated based on cylinder hydraulic diameter, $D_h = 4A_c/P$. The runs are carried out at constant heat flux condition using air as a fluidizing gas.

Table 1. Properties of phases used in the present simulation

Air properties	
- Density, ρ_a	1.1545 kg/m^3
- Viscosity, μ_a	1.884*10-5 kg/m.s
- Specific heat, CP_a	1007 J/kg ^{o}c
- Thermal conductivity, k_a	0.026606 W/m ^{o}c
- Prandtl number, Pr = μ_a * CP_a / k_a	0.7275
Coal properties	
- Particle mean diameter, d_p	0.002
- Density, ρ_p	354 kg/m^3
- Thermal conductivity, k_p	0.49 W/m ^{o}c
- Specific heat, CP_p	910 J/kg ^{o}c
- Volume fraction	0.6

Table 2. Parameters and boundary conditions used in the present simulation

| Flow type	Laminar
Gas-solid model	Eulerian-Eulerian with KTGF
Wall boundary	No-slip condition for gas, slip condition for solid
Time step	0.00025 S
Convergence criteria	0.001
Under relaxation factors	0.5 for pressure, 0.2 for momentum, volume and granular temperature
Maximum solid packing volume fraction	0.63
Pressure velocity coupling	Simple
Discretization scheme	Second order upwind
Outlet condition	Atmospheric pressure
Superficial gas velocity	0.31, 0.34, 0.37, 0.39. 0.42 m/s
Minimum fluidizing velocity	0.31 m/s
Particle-particle restitution coefficient	0.9
Particle-wall restitution coefficient	0.9
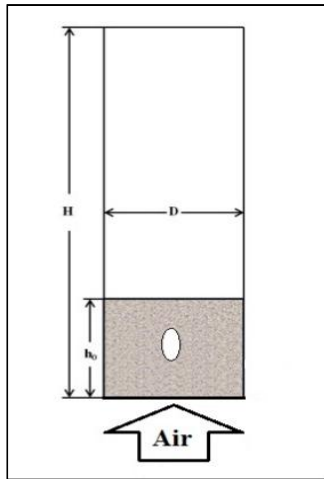
Fig. (1-a). Schematic diagram of the numerical setup

Fig. (1-b). Snapshot of mesh display

5.1 Heat Transfer

The local heat transfer coefficients are taken close to the tube within the reactor of the single tube simulation at 6 s around the tube surface. Fig. (2) shows the predicted local Nusselt number distribution around the tube circumference for the molecular thermal conductivity. For the range of gas velocity considered, at minimum fluidization velocity, Re = 914, the Nu_θ is maximum at the sides of the cylinder and minimum at the stagnation, $\theta=0^o$, and top, $\theta=180^o$, of the cylinder. Minima are found on the top of the tube, where a "stagnant cap" of solids tend to have a long residence time, and around the bottom, where a permanent film of gas is observed to shroud the downward facing surface of the

tube [14]. At higher gas velocities, Re ≥1262, the maximum coefficient is predicted to move around to the top, around the ±135° position, of the tube due to the regular dislodgement of particles there and more frequent contact of the upper tube surface with particles, as compared to the sides and bottom [15]. All curves for in between Reynolds numbers provide similar trends but different magnitudes. Generally, this figure shows that the local Nusselt number is increased with the increasing the Reynolds number.

Effect of gas velocity on the average Nusselt Number, based on particles diameter, Nup, at different (U_{sup}/U_{mf}) for single tube is shown in Fig. (3).The predicted average Nusselt Number increases, Nu_p, as (U_{sup}/ U_{mf}) increase. Since there is no available data about elliptic cylinder immersed in fluidized bed, the present data is compared with the correlation proposed by Gelperin et al [16] for a circular cylinder as shown in Fig. (3). It can be seen that, a reasonable deviation about 11-30% is found, and it may be attributed to the change in operating conditions in addition to different tube cross section.

5.2 Volume Fraction of Solid

The gas fluidized bed reactor is modelled with single horizontal heated immersed tube. The contour plots of the particle volume fraction within the reactor are displayed through the 6.0 seconds in Fig. (4). These contours of volume fractions of pulverized coal and air in the reactors obtained at air velocity of 0.42 m/s for initial static bed height 0.25 m after the quasi steady state is achieved. The colour scale given to the right gives the value of volume fraction corresponding to the colour. Fig. (4) shows the variation in the bed profile with time for solid phase. The fluidized bed profile changes with time till there is no significant change in bed profile which indicates that the fluidized bed reached in a quasi-steady state. Once the fully developed quasi-steady state is reached, then calculate the averaged quantities in terms of time, axial and radial direction. It can be observed that, in the early stages, a collection of air below the tube forms. A larger air bubble is formed and ascends through the bed with time starting from the inlet while the small air voidage under the tube continues up blanketing round the tube. At 0.5 S, this voidage leaves the tube to continue up across the mixture while the larger bubble reaches the tube and begins to cover the tube. As expected, the presence of large bubbles

within the bed causes a higher bed height expansion which is seen in Fig. (4) at 0.25–1 S. Once the bed dynamics have been established these small bubbles continue with similar sizes resulting in little variation in bed height.

5.3 Velocity Vectors

The velocity vectors are helpful in determining flow patterns in fluidized bed. Fig. (5) shows the velocity vectors of air and pulverized coal in the fluidized bed reactor obtained at minimum fluidization velocity for initial static bed height 0.25 m and particles of diameter size 2 mm after the quasi steady state has been achieved. From the vector of solids it can be seen that, there is a small length vigorous movement of the solid particles at the bottom part of the bed. In the upper part of the fluidizing section, there is a circulatory motion of the particles with movement near the wall in the downward direction while that
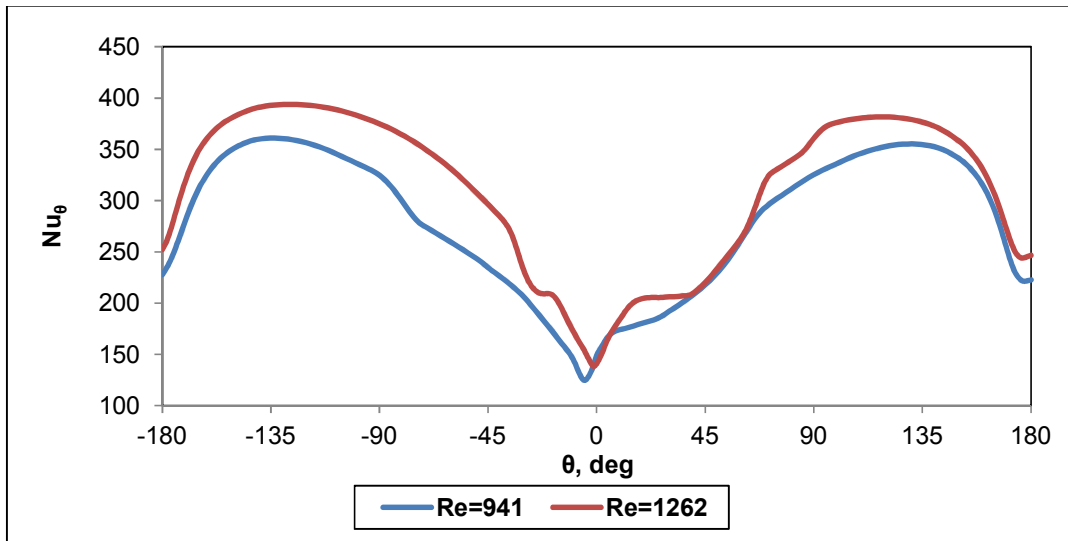

Fig. 2. Local predicted Nusselt number at 6 s versus circumferential location θ, deg for the full circumference of the immersed tube comparing to the Re
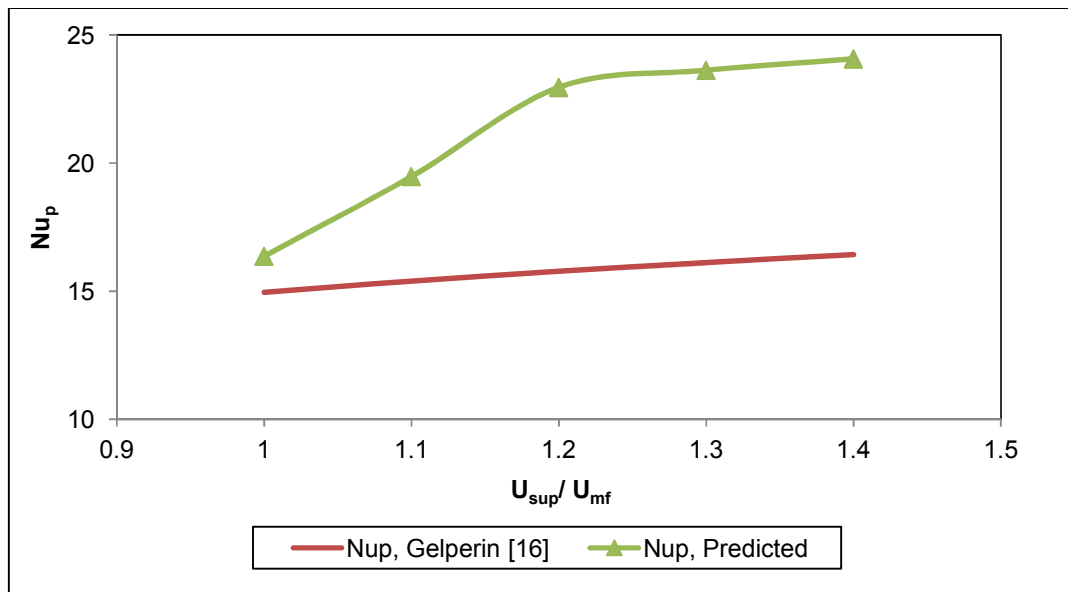

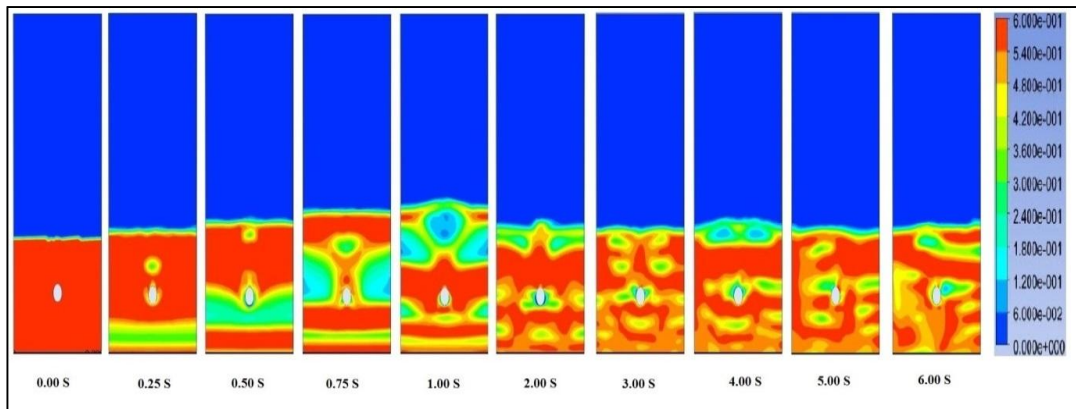**Fig. 3. Predicted average Nusselt number, Nu$_p$, versus fluidization number, U$_{sup}$/U$_{mf}$**

Fig. 4. Contours of solid volume fraction of 2 mm mean diameter at air velocity of 0.44 m/s with respect of time for initial bed height 0.25 m
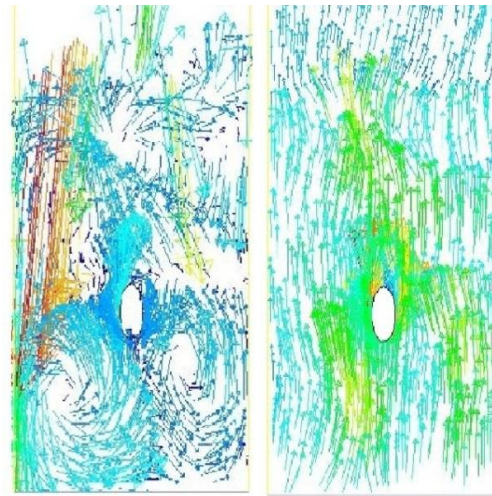

Fig. 5. Velocity vector of air and solid respectively, in FBR of single tube

in the central zone is upward. But in case of the air velocity vector inside the column shows an upward trend. However, the velocity is higher in fluidized part of the bed if compared with the no solids part of the column. This is because less space is available for air to flow between bed particles and tubes.

6. CONCLUSION

The heat transfer characteristics and flow patterns around elliptic cylinder immersed in fluidized bed of pulverized coal were studied numerically with air as a fluidizing gas. A numerical set-up was designed using CFD, 2-D, ANSYS 14.5, TFM, Eulerian-Eulerian with KTGF to predict the heat transfer and bed hydrodynamics of pulverized coal. The simulation results of the present study showed that, for the

range of gas velocity considered, at minimum fluidization velocity, Re = 914, the Nu_θ is maximum at the sides of the cylinder and minimum at the stagnation, $\theta=0^o$, and top, $\theta=180^o$, of the cylinder. The average Nusselt number for the elliptic cylinder increases with the increase of the Reynolds number.

COMPETING INTERESTS

Authors have declared that no competing interests exist.

REFERENCES

1.   Kuipers JAM, Van Duin KJ, Van Beckum FPH, Van Swaaij WPM. A numerical model of gas-fluidized bed. Chemical engineering science. 1992;47(8):1913-1924.

2.	Gustavsson M, Almstedt AE. Numerical simulation of fluid dynamics in fluidized beds with horizontal heat exchanger tubes. Chemical engineering science. 2000;55: 857-866.

3.	Yusuf R, Melaaen MC, Mathiesen V. CFD modeling of heat transfer in gas fluidized bed. Fourth international conference on CFD in the oil and gas, Metallurgical & Process Industries, SINTEF/ NTNU, Trondheim, Norway; 2005.

4.	Wankhede US, Adgulkar DD. CFD simulations of heat transfer in a bubbling fluidized bed for different materials. First international conference on emerging trends in engineering and technology. 2008;1094-1098.

5.	Zhao YZ, Yu AB, Zulli P. A new computational method for studying heat transfer in fluid bed reactors. Powder technology. 2010;197:102-110.

6.	Armstrong LM, Gu S, Luo KH. The influence of multiple tubes on the tube-to-bed heat transfer in a fluidized bed. International Journal of multiphase flow. 2010;36:916-929.

7.	Teaters L. A computational study of the hydrodynamics of gas-solid fluidized beds. M. sc. Thesis, Mechanical engineering, Virginia polytechnic institute and state university, (Virginia Tech); 2012.

8.	Perrone D, Amelio M. A preliminary study of hydrodynamics and heat transfer in a bubbling fluidized bed containing sand particle using CFD. 69th conference of the Italian thermal machines engineering association, ATI2014, Energy Procedia. 2015;81:1041-1054.

9.	Schmidt A, Renz U. Eulerian computation of heat transfer in fluidized beds. Chemical engineering science. 1999;54:5515-5522.

10.	Gan J, Zhou Z, Yu A. Particle scale study of heat transfer in packed and fluidized beds of ellipsoidal particles. Chemical Engineering Science. 2016;144:201-215.

11.	Wahyudi H, Chu K, Yu A. 3D particle-scale modeling of gas–solids flow and heat transfer in fluidized beds with an immersed tube", International Journal of Heat and Mass Transfer. 2016;97:521–537.

12.	Li Z, Janssen TCE, Buist KA, Deen NG, van Sint Annaland M, Kuipers JAM. Experimental and simulation study of heat transfer in fluidized beds with heat production. Chemical Engineering Journal. 2017;317:242-257.

13.	Syamlal M, O'Brien TJ. Computer simulation of bubbles in a fluidized bed. AIChE Symposium Series. 1989;85:22-31.

14.	Tan Z, Guo Z, Yang J, Wang Q. Numerical investigation of heat transfer for elliptical tube in granular flow using DEM. Energy Procedia. 2019;158: 5504-5509.

15.	Chandran R, Chen JC, Staub FW. Local heat transfer coefficients around horizontal tubes in fluidized beds. AIChE J. 1980;102(2):152–157.

16.	Gelperin NI, Kruglikov VY, Ainshtein VG. Heat transfer between a fluidized bed and the surface of a single tube in longitudinal and transverse gas flow (in Russian), Khim. Prom. 1958;6:358.

Peer-review history:
The peer review history for this paper can be accessed here:
http://www.sdiarticle4.com/review-history/52851